

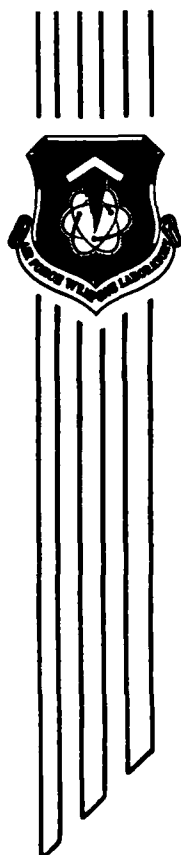
2

AD-A144 595

**PLASMA CONDUCTIVITY EXPERIMENTS  
ON PULSED HIGH-VOLTAGE DISCHARGES  
BY TWO COIL RF-PROBE**

Kyle J. Hendricks, et al.

July 1984



**Final Report**

Approved for public release; distribution unlimited.

DTIC FILE COPY

DTIC  
ELECTE  
AUG 21 1984  
S B  
A

**AIR FORCE WEAPONS LABORATORY  
Air Force Systems Command  
Kirtland Air Force Base, NM 87117**

84 08 20 184

This final report was prepared by the Air Force Weapons Laboratory, Kirtland Air Force Base, New Mexico, under Job Order 57972202. Lieutenant Kyle J. Hendricks (NTYP) was the Laboratory Project Officer-in-Charge.


When Government drawings, specifications, or other data are used for any purpose other than in connection with a definitely Government-related procurement, the United States Government incurs no responsibility or any obligation whatsoever. The fact that the Government may have formulated or in any way supplied the said drawings, specifications, or other data, is not to be regarded by implication, or otherwise in any manner construed, as licensing the holder, or any other person or corporation; or conveying any rights or permission to manufacture, use, or sell any patented invention that may in any way be related thereto.

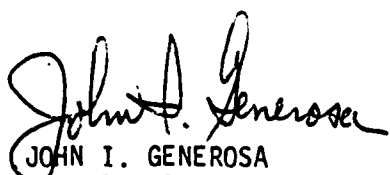
This report has been authored by an employee of the United States Government. Accordingly, the United States Government retains a nonexclusive, royalty-free license to publish or reproduce the material contained herein, or allow others to do so, for the United States Government purposes.

If your address has changed, if you wish to be removed from our mailing list, or if your organization no longer employs the addressee, please notify AFWL/NTYP, Kirtland AFB, NM 87117 to help us maintain a current mailing list.

This report has been reviewed by the Public Affairs Office and is releasable to the National Technical Information Service (NTIS). At NTIS, it will be available to the general public, including foreign nations.

This technical report has been reviewed and is approved for publication.

  
KYLE J. HENDRICKS  
Lieutenant, USAF  
Project Officer

  
JOHN I. GENEROSA  
Lt Colonel, USAF  
Chief, Simulators & Advanced  
Weapons Concepts Branch

FOR THE COMMANDER  
  
ALAN R. COLE  
Colonel, USAF  
Chief, Advanced Technology Division

DO NOT RETURN COPIES OF THIS REPORT UNLESS CONTRACTUAL OBLIGATIONS OR NOTICE ON A SPECIFIC DOCUMENT REQUIRES THAT IT BE RETURNED.

UNCLASSIFIED

SECURITY CLASSIFICATION OF THIS PAGE

REPORT DOCUMENTATION PAGE				
1a. REPORT SECURITY CLASSIFICATION Unclassified		1b. RESTRICTIVE MARKINGS		
2a. SECURITY CLASSIFICATION AUTHORITY		3. DISTRIBUTION/AVAILABILITY OF REPORT Approved for public release; distribution unlimited.		
2b. DECLASSIFICATION/DOWNGRADING SCHEDULE		5. MONITORING ORGANIZATION REPORT NUMBER(S)		
4. PERFORMING ORGANIZATION REPORT NUMBER(S) AFWL-TR-84-06		7a. NAME OF MONITORING ORGANIZATION		
6a. NAME OF PERFORMING ORGANIZATION Air Force Weapons Laboratory		6b. OFFICE SYMBOL (If applicable) NTYP		7b. ADDRESS (City, State and ZIP Code)
8a. ADDRESS (City, State and ZIP Code) Kirtland Air Force Base, NM 87117		8. PROCUREMENT INSTRUMENT IDENTIFICATION NUMBER		
9a. NAME OF FUNDING/SPONSORING ORGANIZATION		9b. OFFICE SYMBOL (If applicable)		10. SOURCE OF FUNDING NOS.
9b. ADDRESS (City, State and ZIP Code)		PROGRAM ELEMENT NO. 62601F	PROJECT NO. 5797	TASK NO. 22
				WORK UNIT NO. 02
11. TITLE (Include Security Classification) PLASMA CONDUCTIVITY EXPERIMENTS ON PULSED HIGH-VOLTAGE DISCHARGES BY TWO COIL RF-PROBE (U)				
12. PERSONAL AUTHOR(S) Kyle J. Hendricks, M. Collins Clark, Dwight J. Ulrich, L. K. Len				
13a. TYPE OF REPORT Final Report		13b. TIME COVERED FROM Dec 82 TO Jul 83		14. DATE OF REPORT (Yr., Mo., Day) 1984 July
15. PAGE COUNT 40				
16. SUPPLEMENTARY NOTATION channel				
17. COBALT CODES			18. SUBJECT TERMS (Continue on reverse if necessary and identify by block number)	
FIELD	GROUP	SUB. GR.		
14	02		Plasma Conductivity, Conductivity Probe, Two Coil RF-Probe, Electron Beams, Channel Conductivity, Langmuir Probes	
20	09			
19. ABSTRACT (Continue on reverse if necessary and identify by block number) Experiments directly measuring the plasma conductivity have been done on pulsed, high voltage discharges. The conductivity was measured by a two coil RF-probe and verified using conventional collecting Langmuir probes. The conductivity measured by these two methods agrees very well. These experiments also demonstrate the potential for the two coil RF-probe to yield useful data in intense electron beam environments.				
20. DISTRIBUTION/AVAILABILITY OF ABSTRACT UNCLASSIFIED/UNLIMITED <input type="checkbox"/> SAME AS RPT. <input type="checkbox"/> DTIC USERS <input checked="" type="checkbox"/>			21. ABSTRACT SECURITY CLASSIFICATION Unclassified	
22a. NAME OF RESPONSIBLE INDIVIDUAL Lt Kyle J. Hendricks			22b. TELEPHONE NUMBER (Include Area Code) (505) 844-0121	22c. OFFICE SYMBOL NTYP

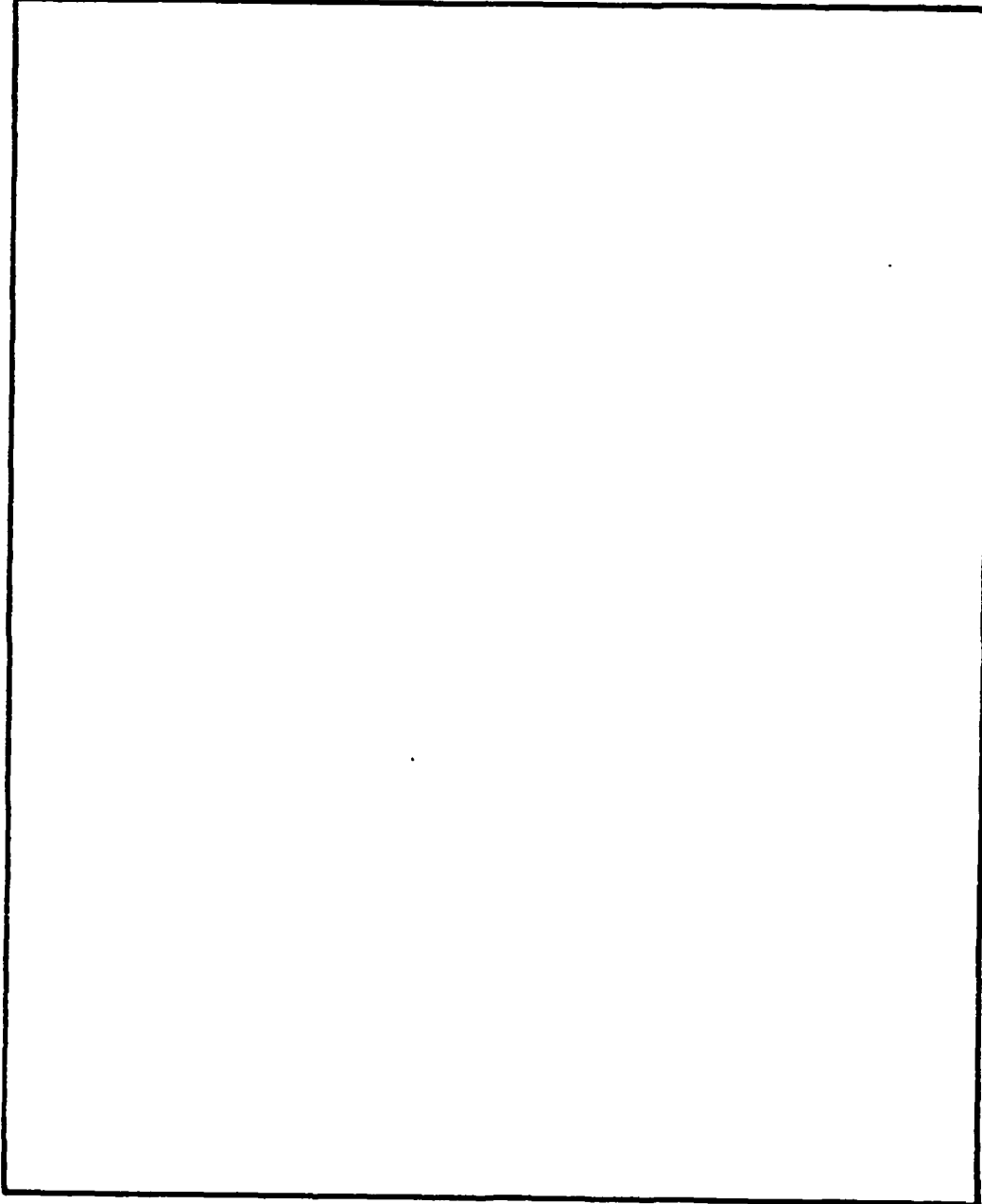
DD FORM 1473, 83 APR

EDITION OF 1 JAN 73 IS OBSOLETE.

UNCLASSIFIED  
SECURITY CLASSIFICATION OF THIS PAGE

UNCLASSIFIED

SECURITY CLASSIFICATION OF THIS PAGE



UNCLASSIFIED

SECURITY CLASSIFICATION OF THIS PAGE

## CONTENTS

<u>Section</u>		<u>Page</u>
I	INTRODUCTION	1
II	THEORY	2
	1. SINGLE PROBES	2
	2. DOUBLE PROBES	4
	3. CONDUCTIVITY	5
	4. TWO COIL RF-PROBE	6
III	EXPERIMENTAL APPARATUS	9
	1. CHAMBERS	9
	2. DIAGNOSTICS	10
IV	DATA	11
	1. LANGMUIR PROBES	11
	2. TWO COIL RF-PROBE	11
V	ANALYSIS	13
	1. LANGMUIR PROBES	13
	2. COILS	14
VI	RESULTS	15
VII	CONCLUSION	16

DTIC  
COPY  
INSPECTED

Accession For	
NTIS GRA&I	<input checked="" type="checkbox"/>
DTIC TAB	<input type="checkbox"/>
Unannounced	<input type="checkbox"/>
Justification	
Distribution/	
Availability Codes	
Avail and/or	
Dist	Special
A-1	

## I. INTRODUCTION

The diagnostics available to obtain measurements on the conductivity channel which forms around a relativistic electron beam presently only give indirect observation (e.g., the magnetic dipole decay time). A useful diagnostic would give you a direct measure of the conductivity and also a temporal variation of the conductivity. The experiments discussed in this report deal with developing such a diagnostic.

The completed work is based on experiments as shown in Ref. 1. A two coil RF-probe was used which allowed operation at frequencies near 50 MHz. This development considers a uniform conductivity profile, and the work was extended to include a conductivity profile which had a small radial variation over the diameter of the two coil RF-pobe.

The work included using collecting Langmuir probes as a standard against which the results of the two coil RF-probe were compared. The use of Langmuir probes in the plasmas produced by the high power discharges was not as straightforward as had been anticipated.

This report begins with a discussion of the theory involved in collecting Langmuir probes and the results of the theory. The third section describes the devices and diagnostics used in these experiments. Some typical raw data are presented in Section IV. The method in which the theory is used to analyze the raw data is discussed in Section V. The results are shown in Section VI, and the conclusions are presented in Section VII.

---

1. Mikoshiba, S. and Smy, P. R., Rev. Sci. Instrum., 40, 1187 (1969).

## II. THEORY

The section presents the theory to be used in analyzing the data shown in Section IV. Four areas will be discussed: first, the single Langmuir probe; second the double Langmuir probe; third, the conductivity measured by the single and double Langmuir probes; and fourth, the two coil RF-probe.

### 1. SINGLE PROBES

The single probe allows the current to be collected and measured by a probe of area  $A$ , as a function of applied voltage. This voltage is applied between the probe and a large reference electrode, typically the defined ground of the system. The current collected by the probe is a sum of all the currents due to the different species of the plasma. For the devices discussed here there are two species of electrons: (a) the Maxwellian plasma, and (b) the super-thermal electrons produced by the machine discharge. There is an ion contribution to the current, which is usually much smaller than either electron species component, typically observed when the probe is biased negatively.

Reference 2 discusses a Langmuir characteristic (I-V curve) which shows the effects of two electron distributions of different temperature ( $T_e$ ). This discussion leads to a semiempirical equation describing a Langmuir characteristic for a planar probe of area ( $A$ ) and voltages ( $V$ ) less than the local space potential ( $\phi_p$ ). The equation is not valid for voltages greater than the space potential because the probe area becomes a function of voltage as the Debye length increases. The equation is:

$$I = A + B \times V + C \times e^{\frac{V}{T_e}} \quad (1)$$

where  $A$  shows the ion contribution,  $B$  the contribution due to the superthermal electrons, and  $C$  the Maxwellian plasma contribution. The factor  $C$  is an unknown only because the plasma saturation current  $I_{pe}$  is not known initially. The  $C$  can be explicitly written:

- 
2. Chen, F. Plasma Diagnostic Techniques ed. by R. H. Huddleston and S. L. Leonard, Academic Press (1965).

$$C = I_{pe} \times e \frac{-\phi_p}{T_e} \quad (2)$$

This discussion allows the various plasma parameters to be determined: density in  $\text{cm}^{-3}$ ,  $\phi_p$  in volts (V), and  $T_e$  in electron-volts (eV).

There is a basic relation from statistical mechanics between the plasma saturation current  $I_{pe}$ , plasma density  $n$ , plasma electron temperature  $T_e$ , and probe area  $A$  which is:

$$I_{pe} = e \langle nv \rangle A \quad (3)$$

The quantity  $\langle nv \rangle$  is the averaged flux density for the specific species, in this case the plasma electrons. The average flux density for a single probe has been shown to be (Ref. 2):

$$\langle nv \rangle = \frac{n \times v_{th}}{\sqrt{2\pi}} \quad (4)$$

where  $v_{th}$  is the electron thermal velocity in cm/s (Ref. 3).

Inserting Equation 4 into Equation 3 and solving for the density as a function of  $I_{pe}$  and  $T_e$  we find:

$$n = \delta \frac{I_{pe}}{\sqrt{T_e}} \quad (5)$$

where  $\delta = 5.8 \times 10^8$  when a 1/4 in diameter disc probe is used to measure the current, and  $I_{pe}$  in mA and  $T_e$  in eV.

The discussion of the conductivity calculation from Langmuir probe data will be deferred until the double Langmuir probes are discussed.



## 2. DOUBLE PROBES

Double collecting Langmuir probes are typically used in plasmas without a large reference electrode. However, double probes have an interesting feature in that they remain at the plasma floating potential. This feature makes double probes useful in high potential discharges. The single probe must be swept in voltage through the local space potential, however, the double probe never needs knowledge of the local space potential and in fact is unable to determine the local space potential. Refer to References 2 and 4 for a more complete discussion of the operation of double probes.

By keeping the double probe at the floating potential, the current collected by one side of the double probe is limited to the ion saturation current. The current drawn as a function of the relative bias  $V$  across the two electrodes can be written (Ref. 2):

$$I = I_{pi} \tanh\left(\frac{eV}{T_e}\right) \quad (6)$$

If there are large background signals Equation 6 can be empirically modified to account for such signals, but this will be discussed when we show the analysis of the data.

Then write an equivalent expression to Equations 3 and 4 for double probes:

$$I_{pi} = e \langle nv \rangle A_t \quad (7)$$

where:

$$\langle nv \rangle = \frac{1}{2} n c_s \quad (8)$$

The new quantities are:  $I_{pi}$  the ion saturation current,  $A_t$  the total double probe collecting area,  $c_s$  the ion acoustic velocity (Ref. 3) and the factor  $1/2$  is the Bohm diffusion coefficient. Solving Equation 7 for the density we find:

- 
4. Schott, Plasma Diagnostics ed. by W. Lochte-Holtgraven North Holland Pub. Co. (1968).

$$n = \frac{2 I_{pi}}{e c_s A_t} \quad (9)$$

We now have the plasma ion density, and by requiring quasi-neutrality to infer the electron density, the plasma electron conductivity can be calculated.

### 3. CONDUCTIVITY

The conductivity calculation described in this section applies to both the single and double Langmuir probes discussed previously. The conductivity shown in Krall and Trivelpiece (Ref. 5) is:

$$\sigma = \frac{(\omega_{pe})^2}{4 \pi \nu_c} \quad (10)$$

where  $\omega_{pe}$  is the plasma electron frequency, and  $\nu_c$  is the total momentum transfer frequency of the electrons. The momentum transfer rate includes all collisions with ions, neutrals, and any electric or magnetic field fluctuations. The expression for  $\nu_c$  is:

$$\nu_c = \nu_{ei} + \nu_{en} + \frac{\partial}{\partial t} (\text{fields}) \quad (11)$$

where (Ref. 6)

$$\nu_{ei} = 4 \times 10^{-5} \frac{n}{T_e^{3/2}} \quad (12)$$

$$\nu_{en} = 5.5 \times 10^8 p_0 (T_e)^{3/2} \quad (13)$$

with  $n$  and  $T_e$  defined above and  $p_0$  is the neutral gas pressure in torr.

In  $\nu_c$  the electron-neutral collision term is the dominant momentum loss process in these low fractional ionization plasmas. This term is of the order

---

5. Principles of Plasma Physics by N. A. Krall and A. W. Trivelpiece  
McGraw-Hill Book Company (1973).

6. Milloy, H. B., Crompton, R. W., Keese, J. A., and Robertson, A. G., Aust. J. Phys. 30,61 (1977).

of hundreds of megahertz or tens of nanoseconds time scale. The electron-ion term is an order of magnitude lower in frequency than the electron-neutral loss term and provides only a small part to  $\nu_c$ . The field fluctuation term is comparable in frequency to the RC time of the capacitors which for these experiments is typically tens of microseconds time scale which is steady state compared to the other loss frequencies. Therefore, we neglect the field fluctuation term in  $\nu_c$ .

Substituting Equations 11 through 13 into Equation 10 only parameters computed from the respective characteristic are input. The probe dependent quantities like probe area, bias, or current are not used. These equations are left until they are required in the analysis of the data.

#### 4. TWO COIL RF-PROBE

The development shown in Ref. 1 for the two coil RF-probe is based on the conductivity being a constant out to a radius  $a$ . The theory has been extended to include a slow radial decay out to radius  $a$  which is almost equal to the coil radius  $b$ . This extension will be supported by the conductivity profiles presented later.

The development of the induced voltage signals is well documented (Ref. 1) and will only be summarized here. The starting point is Maxwell's equations with the displacement current term in Ampere's law. Ampere's and Faraday's laws are simultaneously solved for the radial magnetic field. The result is then plugged into Faraday's law for the  $E_\theta$  which in turn leads to an expression for the voltage induced on a search coil of radius  $b$ . This calculation can also be completed for a conducting medium inserted inside the coils, this voltage is defined as  $V$  while the induced voltage without the conductor is called  $V_0$ . The ratio of  $V$  to  $V_0$  is a unique function of the frequency with which you drive the field coil and also the conductivity of the medium in which you are interested. The resulting equation for  $V$  to  $V_0$  is:

$$\frac{V}{V_0} = \frac{J_0[b \sqrt{(m^2 + k^2)}]}{J_1[b \sqrt{(m^2 + k^2)}]} \phi \quad (14)$$

where the function  $\phi$  depends on the product  $\sigma f$ . Symbol  $\phi$  when expanded out looks like:

$$\Phi = \frac{\gamma A J_{1\lambda} + \xi B J_{0\lambda}}{\gamma C J_{1\lambda} + \xi D J_{0\lambda}} \quad (15)$$

where

$$A = J_{1b} Y_{0a} - J_{0a} Y_{1b} \quad B = J_{1a} Y_{1b} - J_{1b} Y_{1a}$$

$$C = J_{0b} Y_{0a} - J_{0a} Y_{0b} \quad D = J_{1a} Y_{0b} - J_{0b} Y_{1a}$$

with

$$J_{0a} = J_0[\gamma a] \quad J_{0b} = J_0[\gamma b]$$

$$J_{1a} = J_1[\gamma a] \quad J_{1b} = J_1[\gamma b]$$

$$Y_{0a} = Y_0[\gamma a] \quad Y_{0b} = Y_0[\gamma b]$$

$$Y_{1a} = Y_1[\gamma a] \quad Y_{1b} = Y_1[\gamma b]$$

$$J_{0\lambda} = J_0[\xi a] \quad J_{1\lambda} = J_1[\xi a]$$

$$\gamma = \sqrt{(m^2 + k^2)} \quad \xi = \sqrt{(m^2 + k^2 - i\lambda^2)}$$

$$m = \alpha + i\beta \quad \alpha \gg \beta \text{ for our work}$$

$$k^2 = \omega^2 \mu \epsilon \quad \lambda^2 = \mu \sigma \omega$$

The J and Y used in these equations are ordinary Bessel and Neumann functions of real or complex argument. The m is the magnitude of the wave vector for  $H_r$  to propagate in the z direction. The factor  $\beta$  shows how the radial magnetic field is attenuated, which is found to be small. Symbol  $\omega$  is the angular frequency of the magnetic field,  $\mu$  is the permeability, and  $\epsilon$  is the permittivity of the conducting medium. The quantity  $\lambda^2$  shows the explicit dependence of  $V/V_0$  on the conductivity.

This set of equations allows a unique determination of  $V/V_0$  for a given value of the product  $\sigma f$ . Then by knowing or selecting the frequency  $f$  there is a unique relationship between the conductivity of the medium and the ratio of the induced voltages on the search coils.

## III. EXPERIMENTAL APPARATUS

This section describes the hardware involved in this series of experiments. The section is divided in two parts: first the devices and their mode of operation will be presented, and second the diagnostics and the associated circuitry will be described.

## 1. CHAMBERS

Plasmas were produced for study in three different machines: a coaxial plasma gun (Ref. 4), a glow discharge chamber (Ref. 5), and a capacitor discharged Z-pinch (Ref. 7). The coaxial plasma gun and the associated equipment is shown schematically in Fig. 1. The capacitor bank for the discharge was typically charged to 18 kV by a dc power supply. Initially the trigger pulse for the capacitor discharge was used as a timing mark. This method introduced a very long time delay before the plasma formed between the gun electrodes. The problem was the most noticeable when the neutral gas was puffed into the chamber via the puff valve rather than prefilling to a static pressure  $p_0$ . The timing delay was a result of the flow velocity of the neutral gas and the time required for the gas to breakdown. The jitter in the plasma formation was avoided by using a fraction of the voltage signal from the Rogowski coil (Ref. 4) monitoring the current flow in the gun electrodes. The timing mark from the Rogowski coil gave a stable reference mark in time with which the oscilloscopes could be triggered and record the voltage signals from the probes.

Usually the gun was operated in the prefilled (snowplow) mode where the chamber was prefilled with neutral gas to a static pressure. This mode provides what is called a dense plasma focus on the axis of the gun. This tends to produce a more uniform plasma than when the gun is discharged in the puffed mode.

The timing problems mentioned previously caused us to build a small glow discharge chamber. This chamber produces the plasma by thermionically emitting high energy ( $E \gg T_e$ ) electrons, the superthermal electrons mentioned in the theory section. These electrons have sufficient energy to ionize the

---

7. Len, L. K., PhD Dissertation 1983.

background neutral gas and produce the plasma ions and electrons. This chamber is shown schematically in Fig. 2. Notice magnetic confinement on the plasma was not used. The lack of magnetic fields caused the plasma density and temperature to remain relatively low because the superthermal electrons, and any electrons with several  $T_e$  of energy are rapidly lost to the chamber walls which are at ground potential.

The low density, which in turn means a low plasma conductivity, caused a Z-pinch discharge to be considered in which the density would be a good fraction of what was obtained in the plasma gun. This Z-pinch (Fig. 3) could be operated at much lower capacitor discharge voltages, and the switching and timing would be less of a problem. The Z-pinch was typically operated at 5 kV on six 0.25  $\mu$ f capacitors in parallel. The timing was typically less than a microsecond in variation. The machine provided some important data on the ability of the diagnostics to operate in a pulsed plasma environment.

## 2. DIAGNOSTICS

Two different types of diagnostics were used in the devices discussed in paragraph 1. They were: (a) collecting Langmuir probes, and (b) two coil RF-probe. The Langmuir probes were used to determine the plasma density and electron temperature. The single Langmuir probe was also used to try measuring the local space potential. The double probe was used as a means of getting around the high space potentials associated with capacitor discharges. The circuitry used with the collecting Langmuir probes are shown in Figs. 4a and b. The output signal of the circuits was traced on an oscilloscope and recorded on photographs. The Langmuir probes were made of 5 mil tungsten wire. The probes were inserted into the vacuum in stainless steel support rods, the tungsten was insulated from the stainless by ceramic tubing.

A block diagram for the conductivity probe experiments is shown in Fig. 5. The probe was made of RG-58 coaxial cable mounted on a PVC pipe. The pipe was then bolted directly onto the outer electrode of the plasma gun. The probe was mounted midway between the two electrodes in the capacitor discharge chamber. The conductivity was not large enough in the glow discharge chamber to use the RF-coil probe.

## IV. DATA

The raw data monitored are voltages from the different probes. The voltages from the Langmuir probes are from calibrated current transformers. The voltages from the two coil RF-probe are the output of the oscillator and the differenced signal from the two field coils.

## 1. LANGMUIR PROBES

The data from the single Langmuir probe were recorded as two traces: (a) the current collected as a function of time, and (b) the voltage applied to the probe as a function of time by a Patco pulser. The pulser is designed to output a 300 V pulse in 10 ns and decay back to 0 V in 400 ns (Fig. 6). The output of the pulser was monitored with the current transformer on the low voltage side of the resistor in Fig. 4a. The current drawn by the probe for the bias at a given time is monitored by the current transformer on the high voltage side. Typical voltage signals from these transformers are shown in Figs. 7a and b.

The data analyzed in the next section came from the decaying voltage part of the pulse. The falling end was used to achieve better time resolution for the Langmuir characteristic.

The data for the double Langmuir probe are again voltage signals from current transformers (Fig. 8). The double probe is set with a fixed bias for a given shot. A series of shots was taken to gather sufficient data for a double probe characteristic.

## 2. TWO COIL RF-PROBE

A sample data photograph is shown in Fig. 9a. The figure shows two traces: (a) the upper trace is a double exposure of the oscillator output to insure that the discharge does not change the signal amplitude and cause the calculated conductivity to be wrong, and (b) the lower trace is a double exposure of the search coil signal both before and during the shot. The larger amplitude envelope shows the  $V_0$ , and the smaller amplitude envelope shows the  $V$ .

The oscillator output was monitored because the plasma discharge was observed to perturb the output. The perturbation was found to occur with the



same period as the RC time of the capacitors being used. Since the RC time was a much lower frequency than the coils were being driven, a high pass filter was inserted for signals going from the field coil to the oscillator (Fig. 5).

These referenced data were taken with the oscillator at 25 MHz. The inability to use the two coil RF-probe at frequencies greater than 50 MHz was discussed in Ref 1. Their measurements were repeated to see if the coils could be driven at frequencies greater than 100 MHz. The data recorded are shown in Fig. 10. The data show that for the cases in which the differenced coils or the coils separately were used the coils still could not be driven at frequencies greater than 50 MHz due to the electrostatic coupling between the coils.

## V. ANALYSIS

This section will describe the reduction of raw data discussed in the previous section. The discussion will center on the theory of Section II.

## 1. LANGMUIR PROBES

The raw data of the current and voltage for the single probe were digitized and then the data were cross plotted to obtain the Langmuir characteristic of a single probe (Fig. 11). Equation 1 was then fitted to the characteristic. The subtraction of the ion and primary electron currents from the total current is considered correct when the semilog plot of remaining current versus the probe voltage is linear for voltages less than the local space potential (Fig. 12). The voltage where the semilog plot is discontinuous is defined as the local space potential or plasma potential. The value of the current at the plasma potential is, by definition, the plasma saturation current. The linear semilog plot of current versus voltage has a slope which equals the plasma electron temperature in electron-volts.

Now that the plasma saturation current and electron temperature have been measured Equation 5 can be used to compute the plasma electron density. However, the single probe could not be driven high enough in voltage to measure the plasma saturation current; and the plasma potential could not be measured. Notice that Fig. 11 shows the beginning of the Maxwellian plasma, but the probe is not driven into electron saturation.

The double Langmuir probe was easier to drive into ion saturation and produce the double Langmuir probe characteristic. A series of shots were taken from a given device where the only parameter varied was the bias across the probe wires. For this group of shots the peak value of the current was measured and the current and voltage from a given shot was plotted to generate an experimental double probe characteristic (the dots in Fig. 13). It was observed that the data looked like a hyperbolic tangent function, with the exception that the data did not pass through the origin. Equation 6 was then modified

$$I = I_0 + I_{pi} \tanh \left( \frac{e(V - V_0)}{T_e} \right)$$

Where  $I_0$  and  $V_0$  are offset values to compensate for noise perturbations. The noise perturbations were noticed first in the Z-pinch chamber when the potential across the double probe was kept equal to zero and rotated the double probe about a radius orthogonal to the z axis. The signals showed that the background noise was not a small part of the plasma currents (Fig. 14).

Equation 6 was then inverted to obtain the electron temperature,  $T_e$  for each data point. The effective temperatures were then averaged to obtain a temperature for the set of data. Equation 6 was then graphed over the data points to check for agreement and used the semitheoretical line to obtain the ion density from Equation 9 (line in Fig. 13).

The computed density and temperature from the double probe was used to obtain a local plasma conductivity. The numbers could then be compared between the RF-coils and double probe to check the validity of the methods.

## 2. COILS

The analysis of RF-coils  $V/V_0$  for the conductivity involved numerically evaluating Equation 14. The independent parameters are the frequency and conductivity of the plasma. In evaluating Equation 14 a graph was generated (Fig. 15) which was used to determine the conductivity.

At a given time  $V/V_0$  from Fig. 9 is measured, and then go to the graph of  $V/V_0$  and find the product of  $\sigma f$ , then by knowing the frequency with which the coils are driven the conductivity can be computed. Recall that the oscillator output is monitored during the discharge. This is done so that the  $V_0$  may be adjusted by the proper factor in the event that the plasma loads down the oscillator output and reduces the received signal.

## VI. RESULTS

The analyzed data from the different diagnostics will be discussed. The first item is the radial density profile assumed in using Equation 14 for the conductivity probe. It was found, by using the double Langmuir probe, that the radial density profile of the plasma gun has an e-folding radius on the order of 5 to 6 cm (Fig. 16). The assumption made earlier, then in using the development by Mikoshiba and Smy for a uniform conductivity distribution, seems to agree with the computed conductivity profile in Fig. 17. The local e-folding length for the conductivity is roughly 4 to 5 cm.

The different numerical values for the conductivity found from the two probes is not as poor as anticipated. Better than a factor of 2 agreement is found between the probes. The peak conductivity in the plasma gun is found with the Langmuir probe at a radius of 1 cm is 260 mhos/m, and the peak conductivity is found for the plasma with the two coil probe at 450 mhos/m (Fig. 18). The disagreement may be due to the use of a uniform conductivity model when there is a slow radial decay, or it may be due to the noise perturbations that caused us to use the modified equation to describe the current collected by the double probe. There is one other possible error, and that is the effect of small differences in the areas of the double Langmuir probe. We tend to discount this possibility because the probes are only millimeters in length, but they are definitely not identical.

The principle result being that both the collecting Langmuir (used as a standard) and the RF-coil probe give good agreement on the measured plasma conductivity.

## VII. CONCLUSION

The results presented in the previous section show that the two coil RF-probe can be used in the intense environment of high power discharges. The usefulness of the RF-probe in diagnosing the conductivity channel surrounding relativistic electron beams may require some modification of the probe geometry. There will definitely have to be some kind of isolation of the probe from the driving oscillator and also between the receiver coils and the data recording devices.

The model used to determine the conductivity may need to be changed. For example, the annular conductivity distribution discussed in Ref. 1 may be more appropriate. That question will need to be addressed by the people doing the experiment.

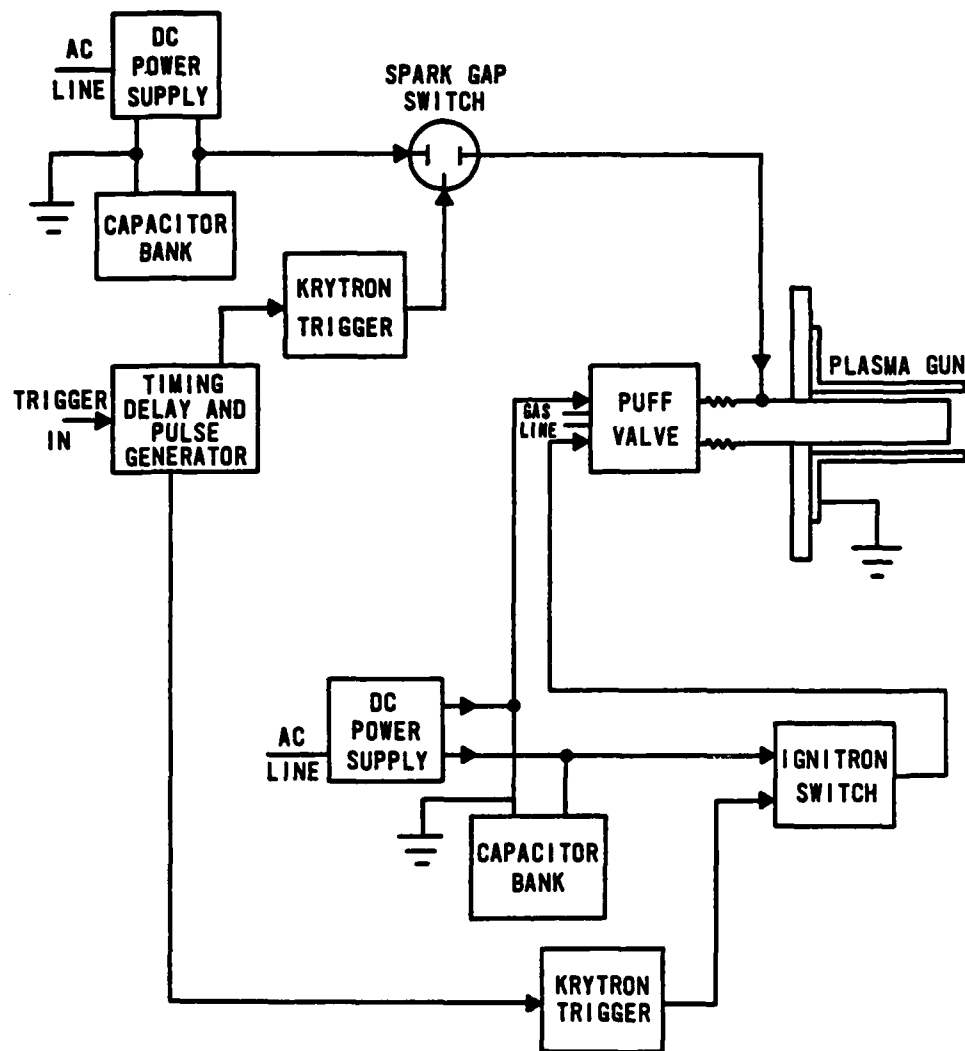


Figure 1. Block diagram of coaxial plasma gun.

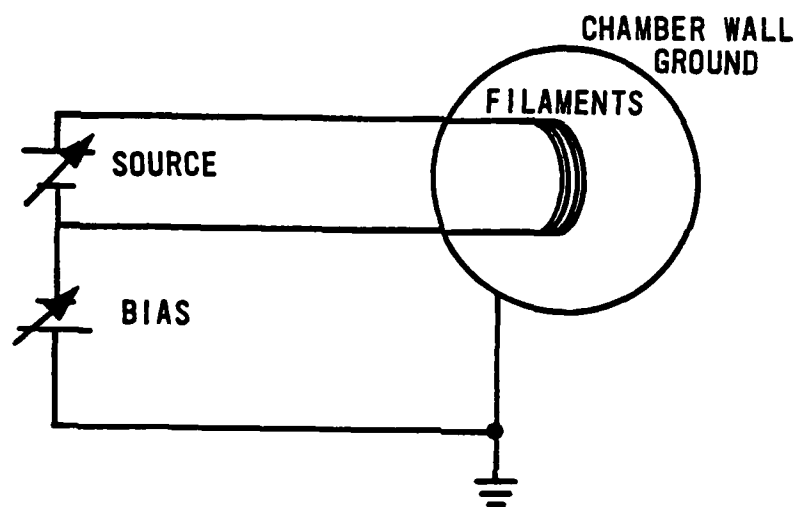


Figure 2. Schematic of glow discharge chamber.

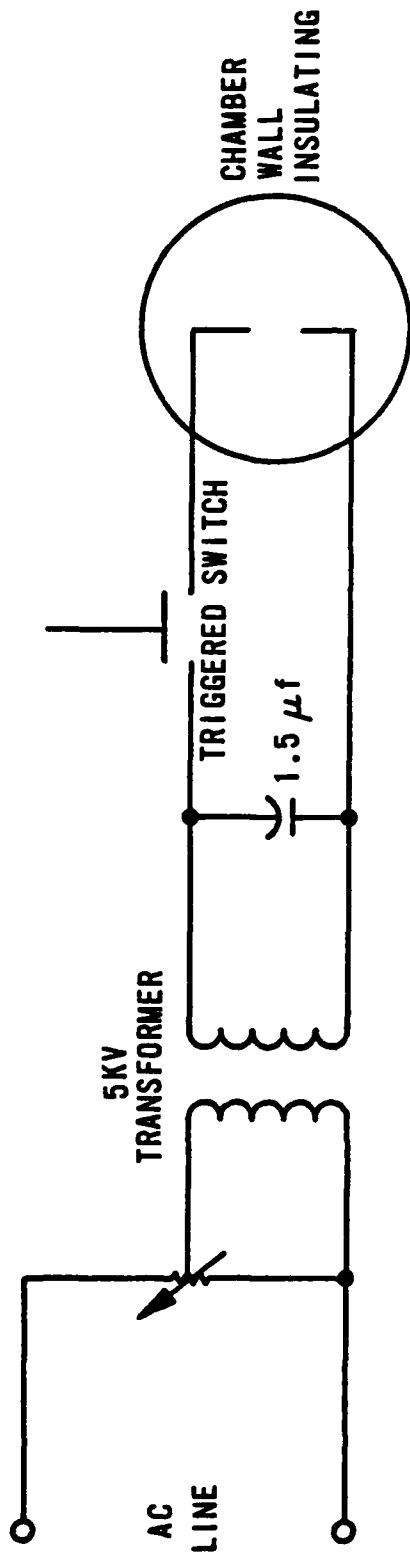


Figure 3. Schematic of pulsed Z-pinch device.



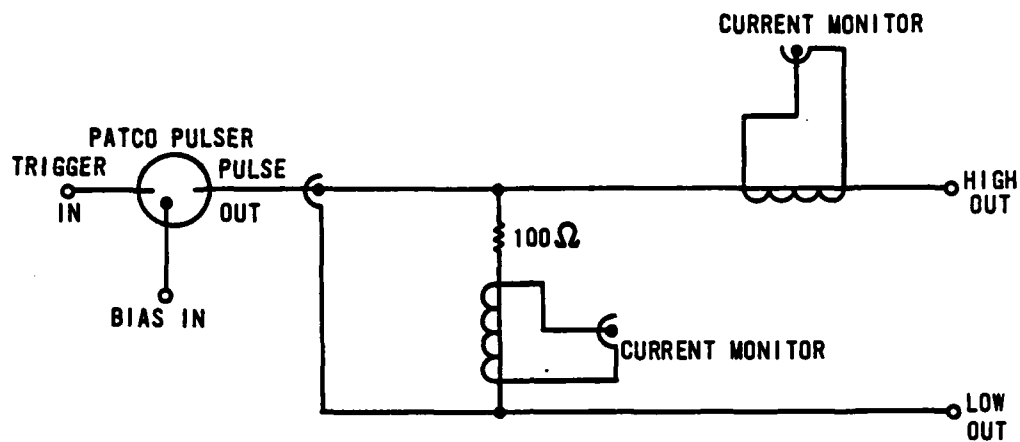


Figure 4a. Schematic of swept single Langmuir probe bias circuit.

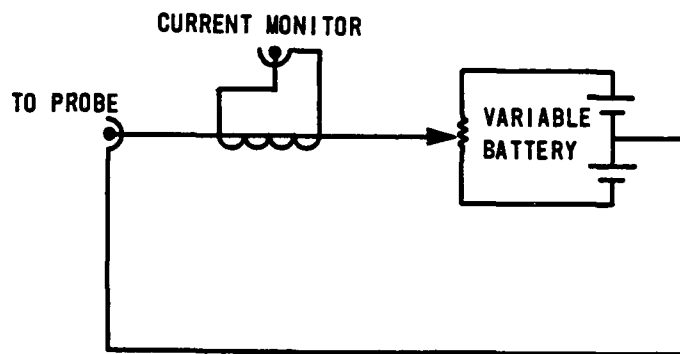


Figure 4b. Schematic of dc-biased double Langmuir probe circuit.

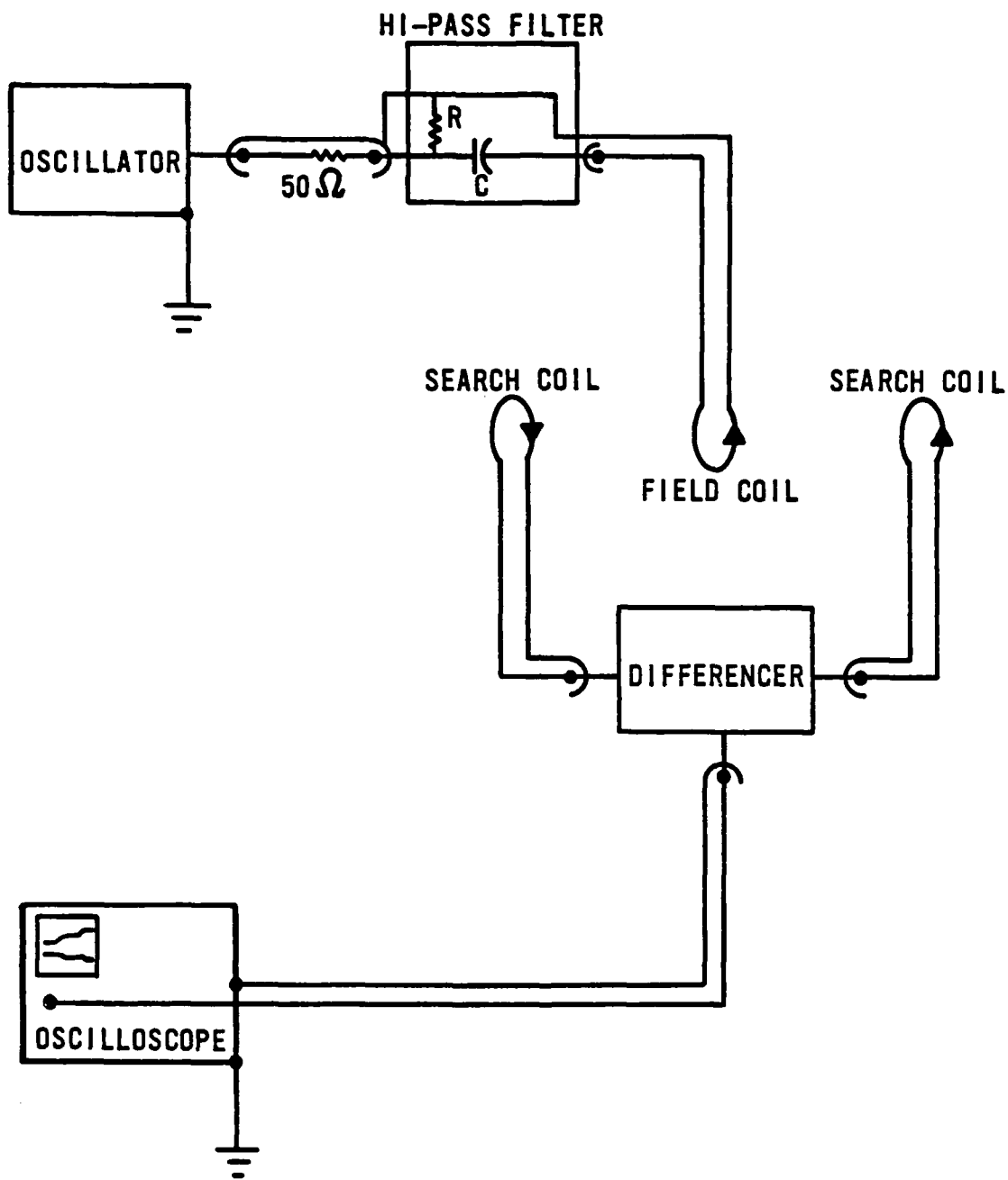


Figure 5. Block diagram of two coil RF-probe diagnostic.

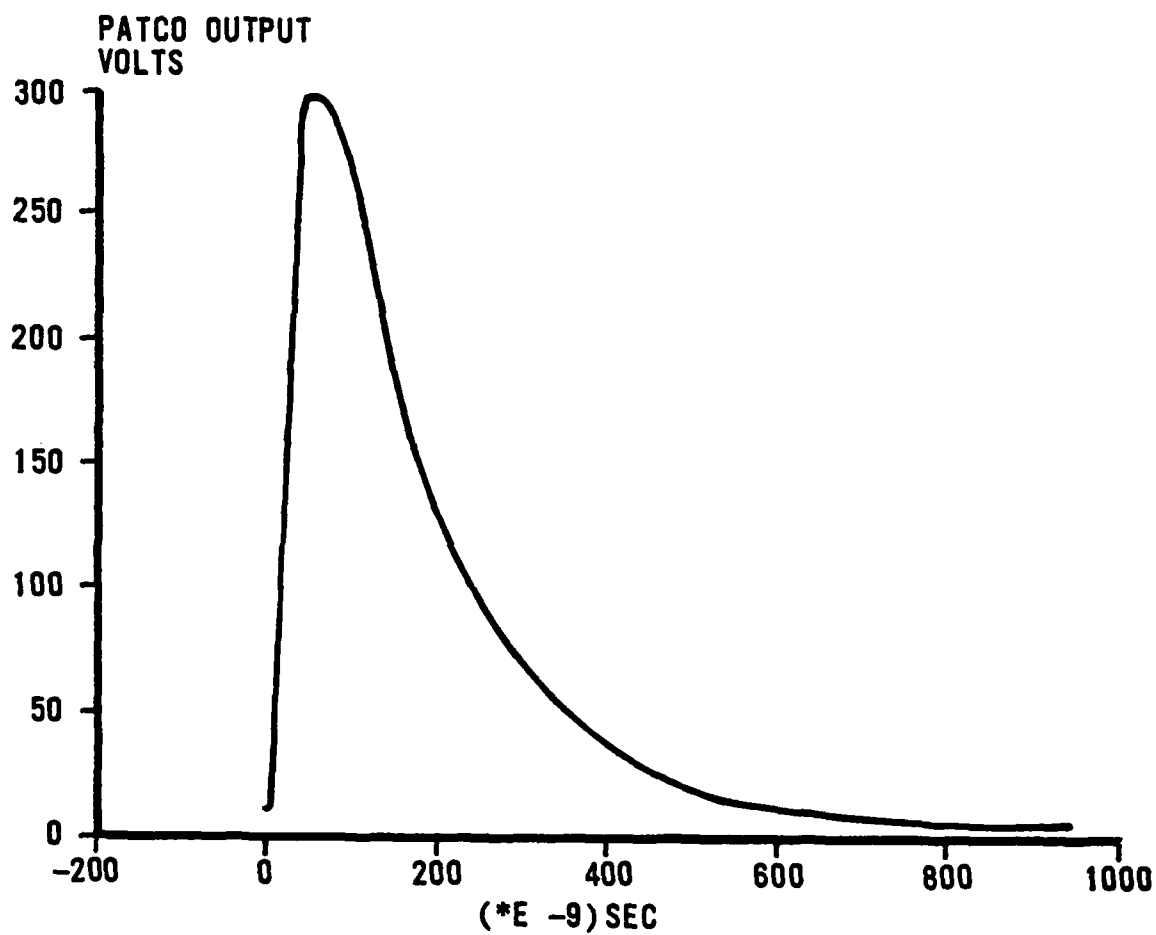


Figure 6. Sample output of Patco pulser used in single Langmuir probe circuit.

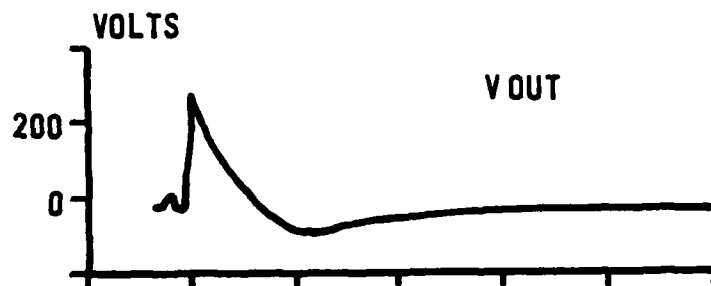


Figure 7a. Sample output from current transformer on low side of 100  $\Omega$  resistor in Fig. 4a.

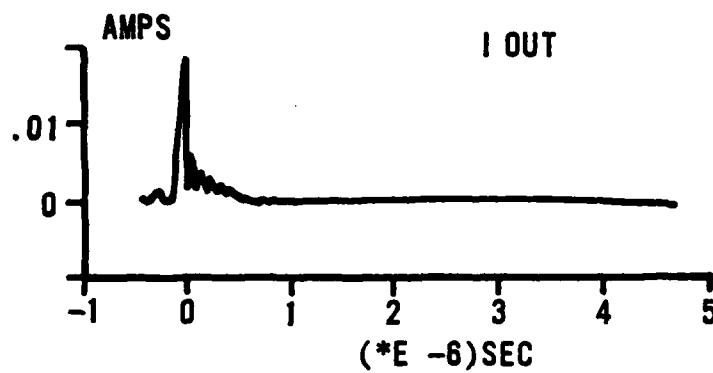


Figure 7b. Sample output from current transformer on high side of 100  $\Omega$  resistor in Fig. 4a.

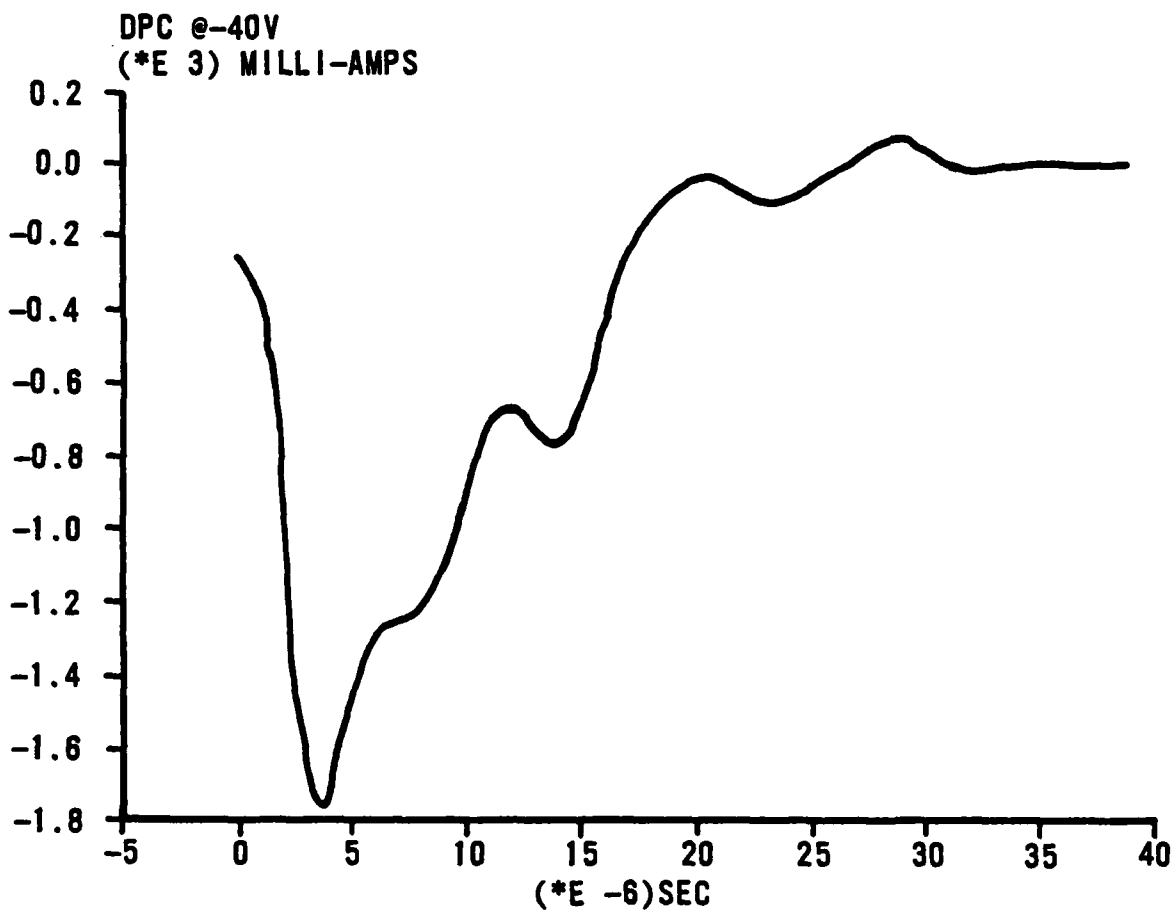


Figure 8. Sample data trace of circuit in Fig. 4b.

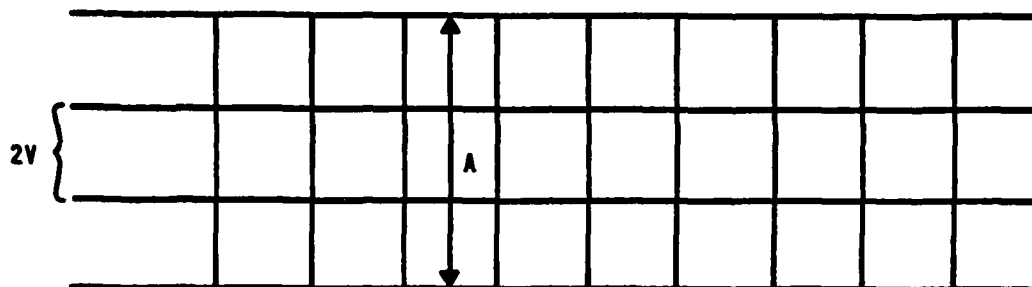


Figure 9a. Double exposure of oscillator output (A) which shows that the discharge does not alter the applied voltage.

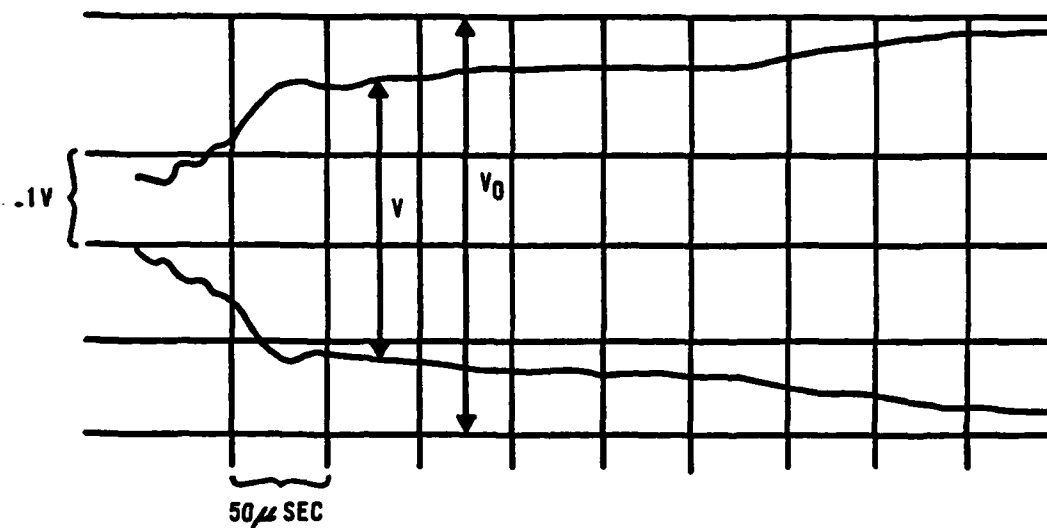


Figure 9b. Double exposure of the differenced search coils showing  $V_0$  and  $V$ .

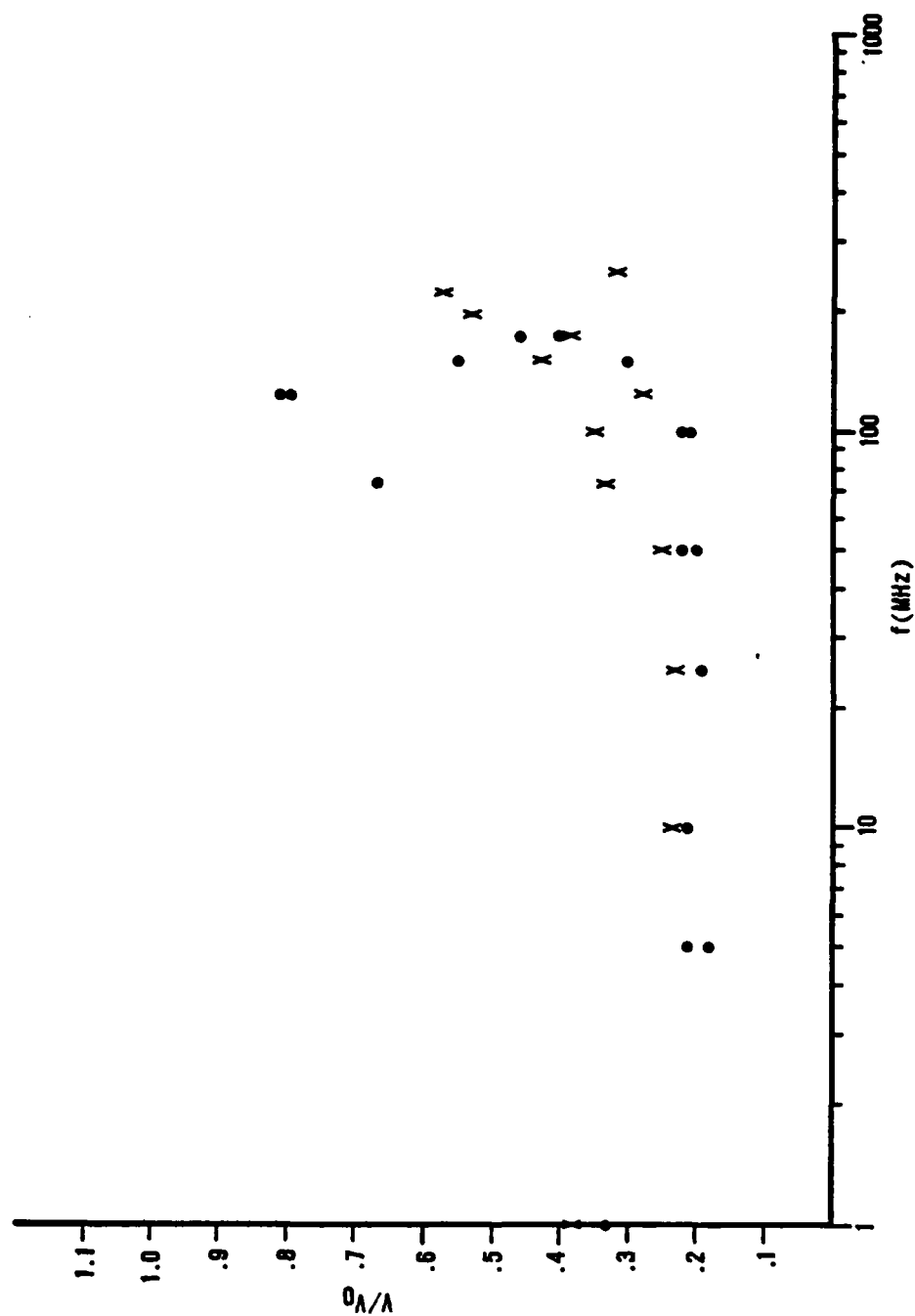


Figure 10. Data showing that the voltages induced on the search coils are mainly due to electrostatic coupling of the coils for  $f > 50$  MHz. (x's are for the differenced search coils, and . 's are for the individual search coils.)

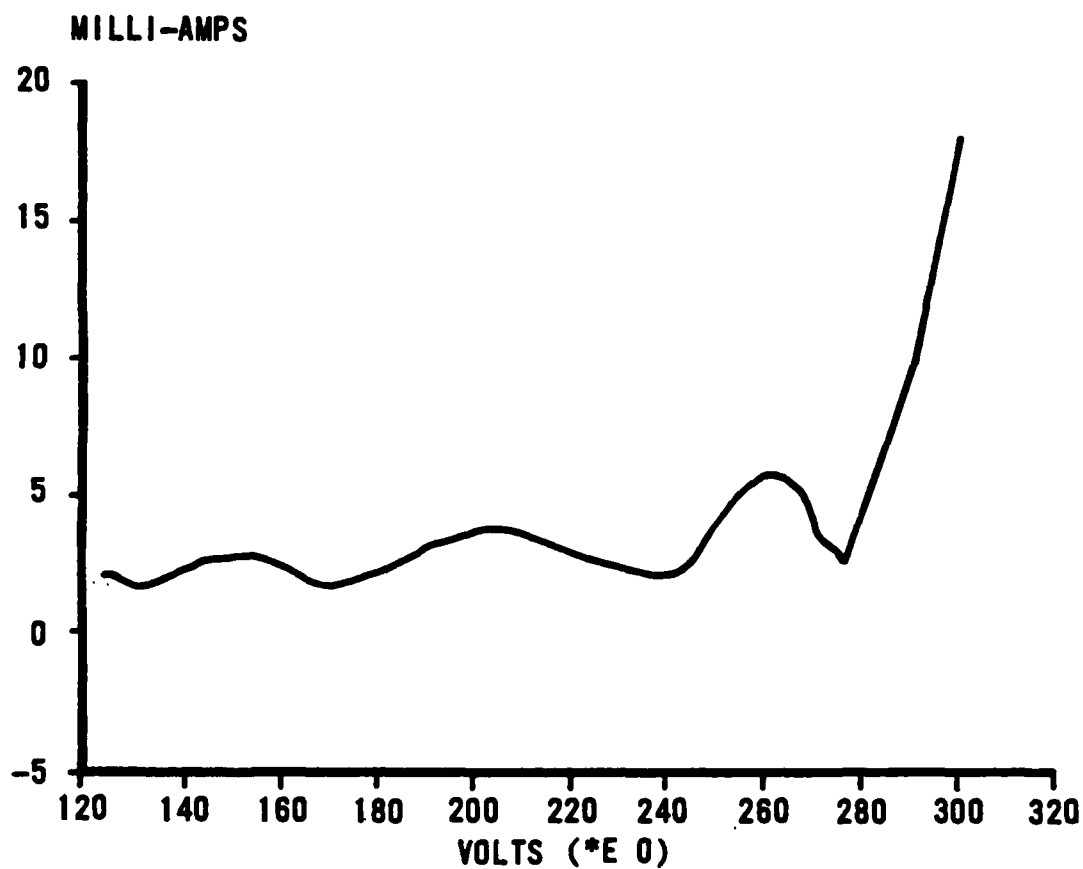


Figure 11. Crossplot of data from Fig. 7a and b.



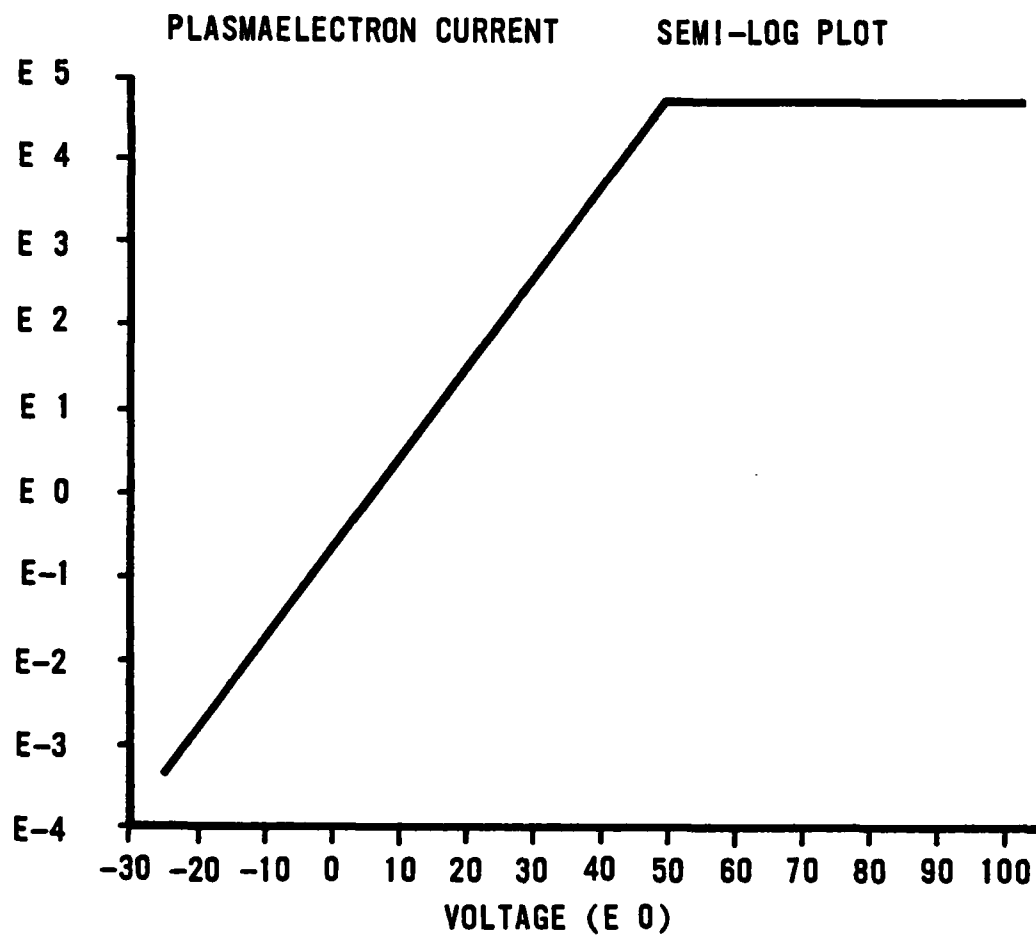


Figure 12. Theoretical plot of  $\ln(I)$  versus  $V$  when the ion and non-Maxwellian electrons have been properly removed from a single Langmuir probe trace.

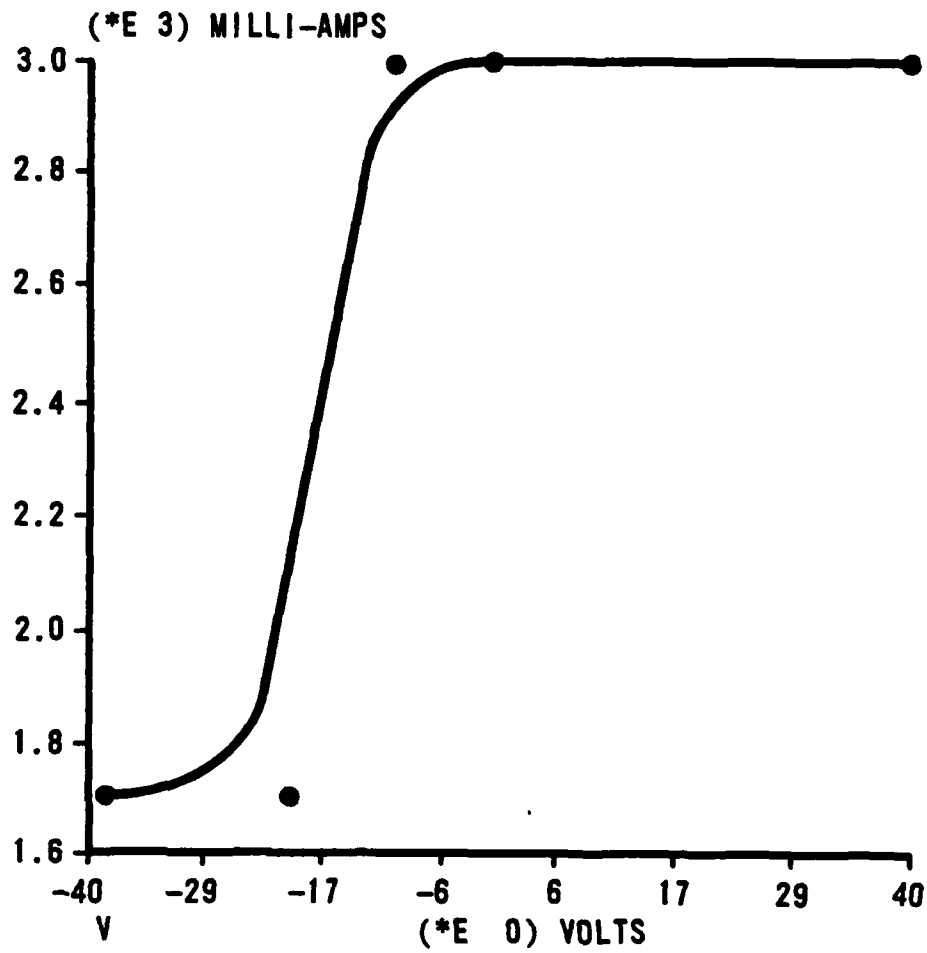


Figure 13. Sample double Langmuir probe trace showing both data (points) and theoretical fit of data (line).

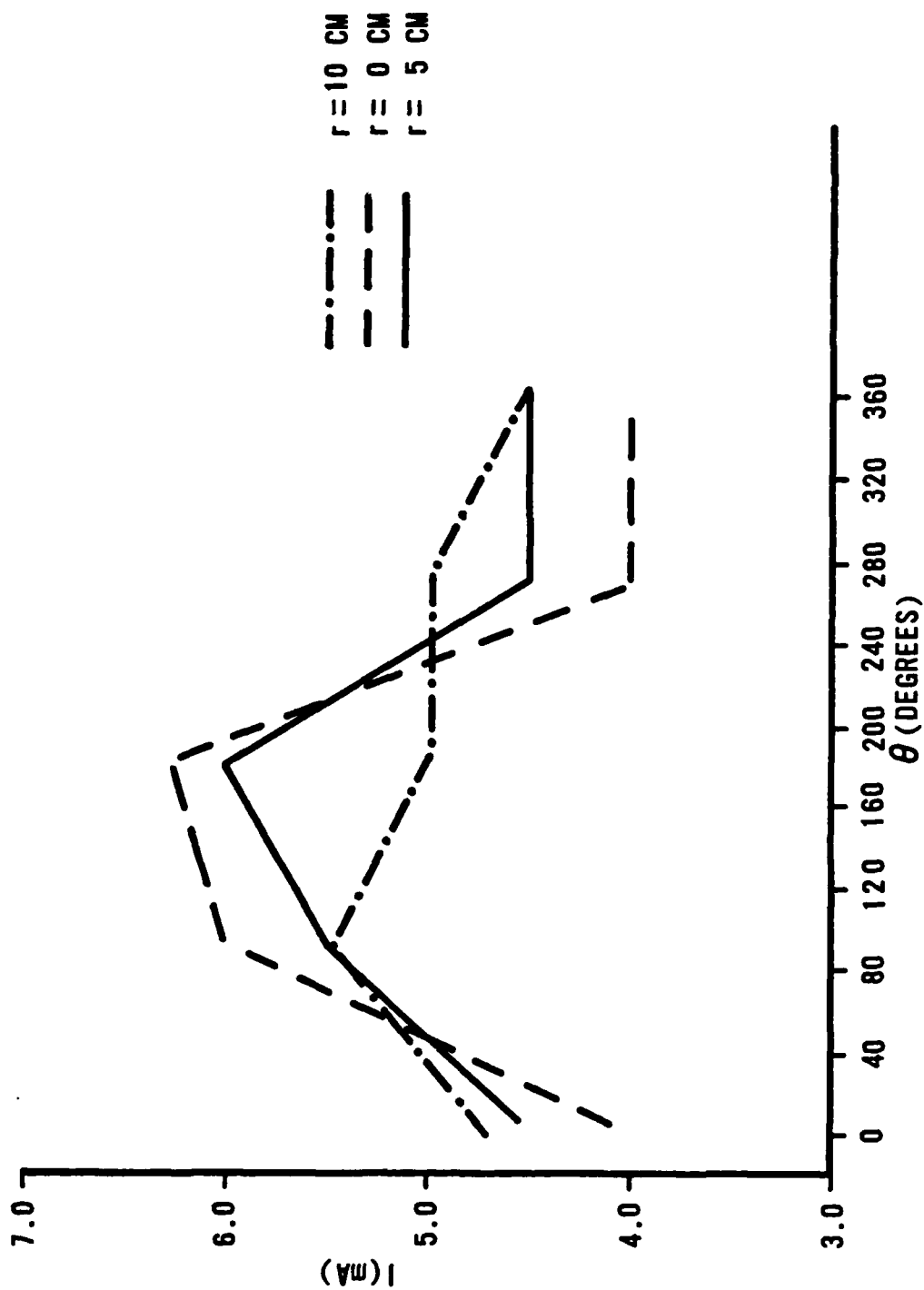


Figure 14. Sample data showing that the noise measured by the double probe is smallest when the plane containing the probe wires is orthogonal to the z-axis ( $\theta = 0$ ).

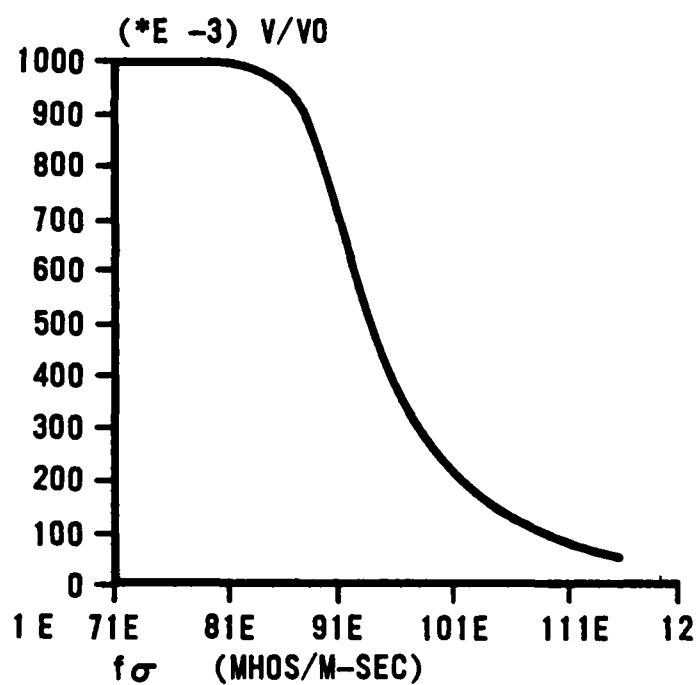


Figure 15. Theoretical plot showing  $V/V_0$  versus  $f\sigma$ .

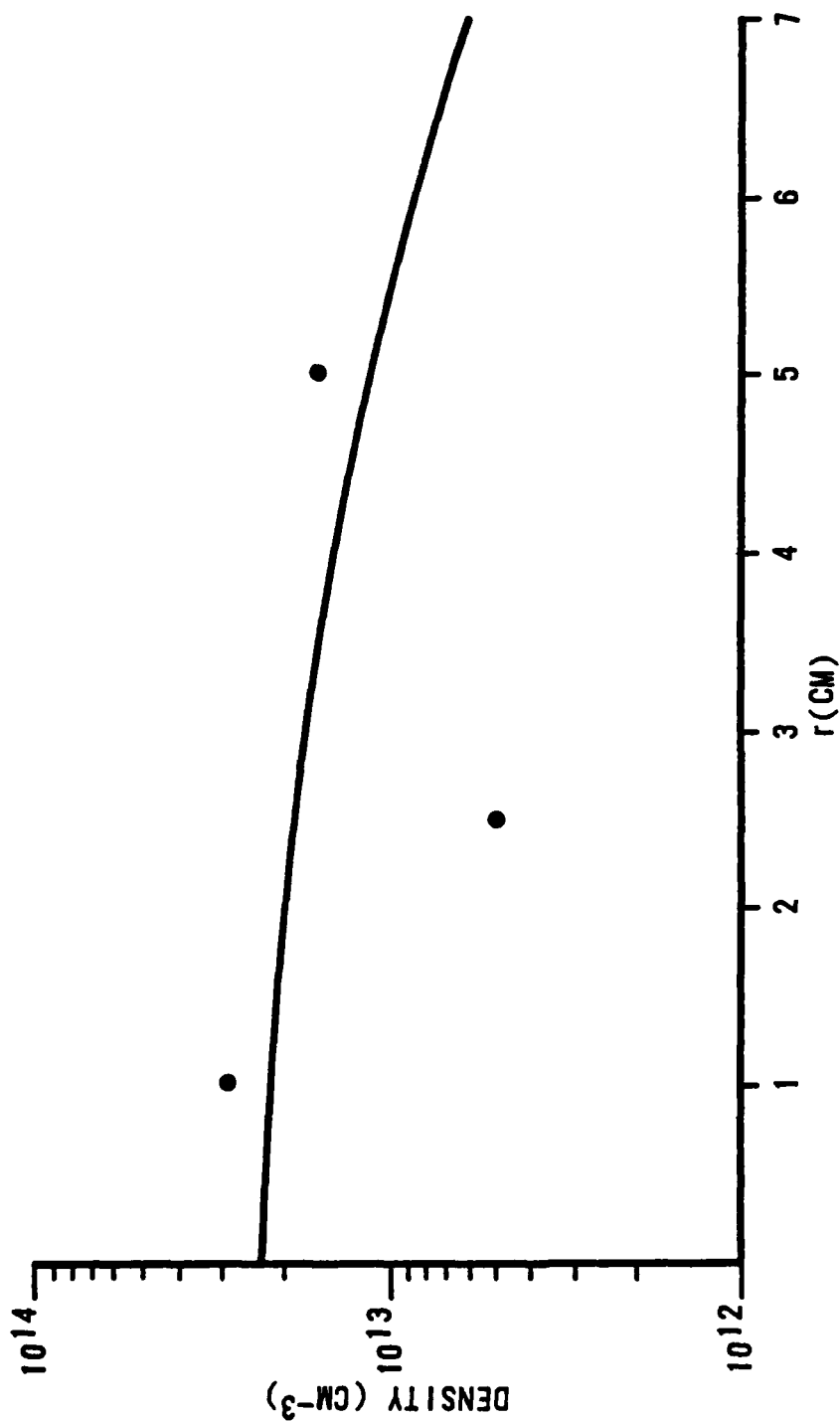


Figure 16. Radial plot of plasma density, determined from a double Langmuir probe characteristic (e.g., Fig. 8).

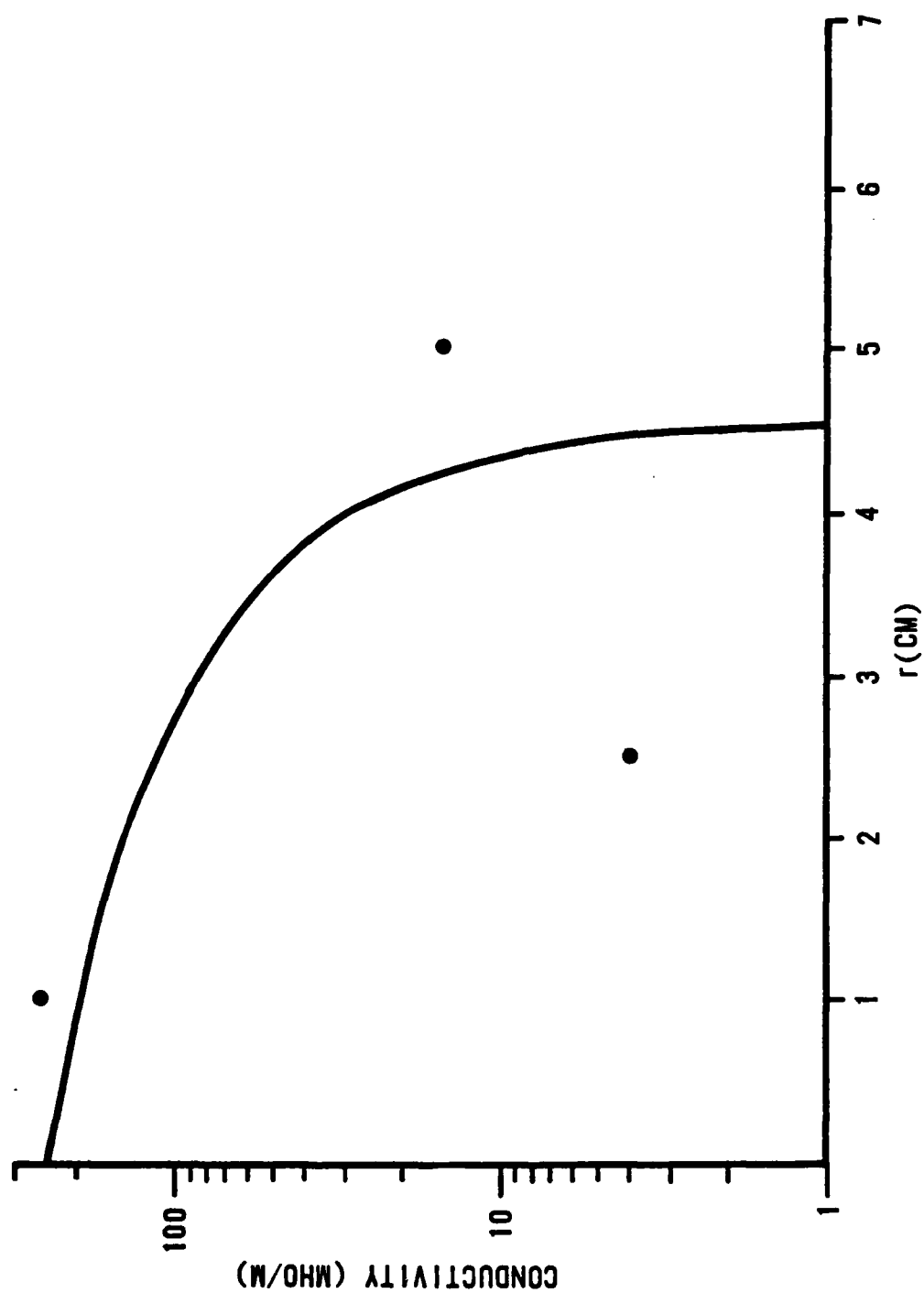


Figure 17. Radial plot of computed conductivity using density and temperature determined using a double Langmuir probe.

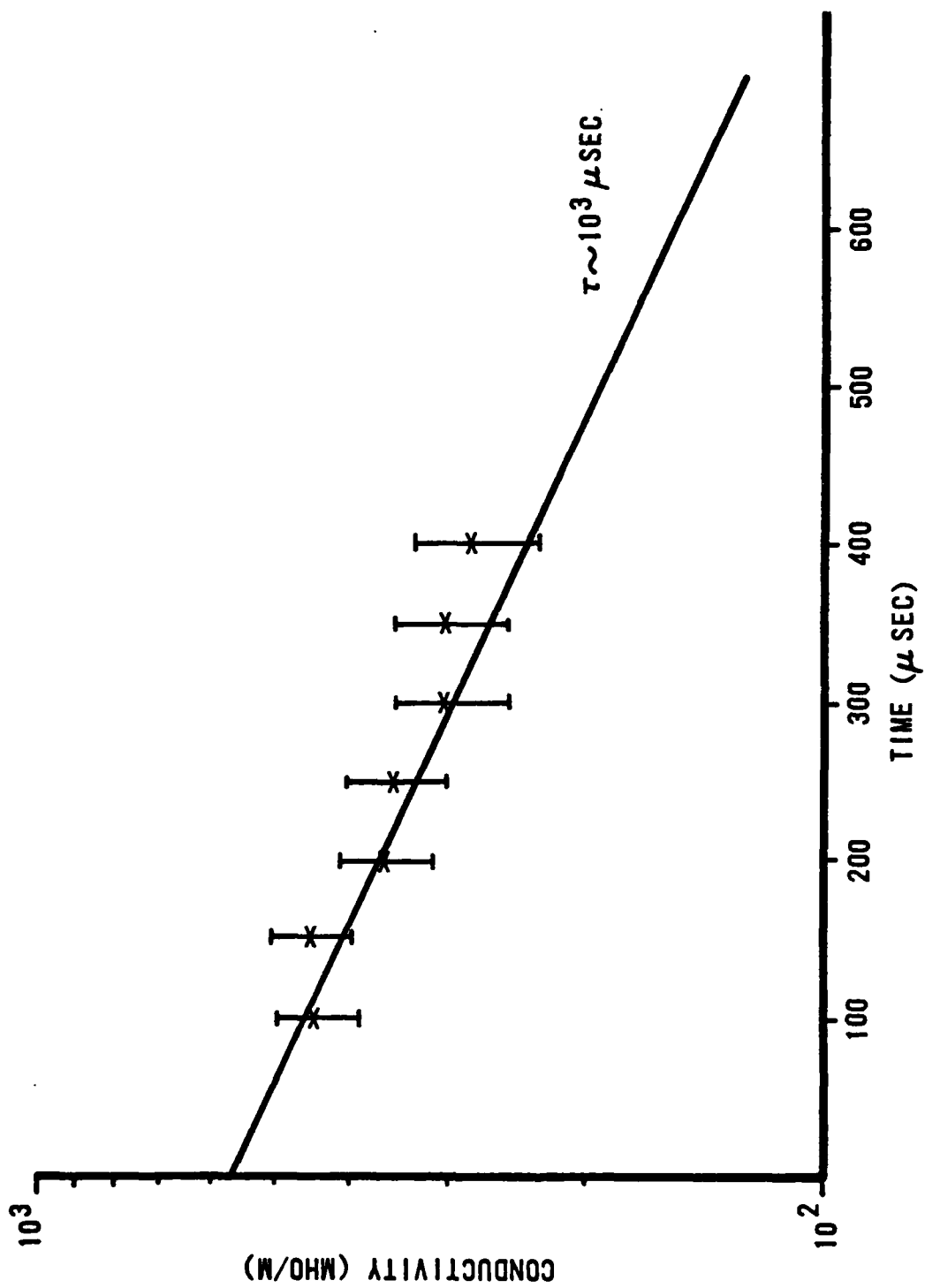


Figure 18. Temporal evolution of conductivity determined from Fig. 9b.